Self-lensing Discovery of a $0.2\,M_\odot$ White Dwarf in an Unusually Wide Orbit around a Sun-like Star[*]

Kento Masuda[1,6] , Hajime Kawahara[2,3] , David W. Latham[4] , Allyson Bieryla[4] , Masanobu Kunitomo[2],
Morgan MacLeod[4,7] , and Wako Aoki[5]

[1] Department of Astrophysical Sciences, Princeton University, Princeton, NJ 08544, USA; kmasuda@astro.princeton.edu
[2] Department of Earth and Planetary Science, The University of Tokyo, Tokyo 113-0033, Japan
[3] Research Center for the Early Universe, School of Science, The University of Tokyo, Tokyo 113-0033, Japan
[4] Center for Astrophysics | Harvard & Smithsonian, Cambridge, MA 02138, USA
[5] National Astronomical Observatory of Japan, 2-21-1 Osawa, Mitaka, Tokyo 181-8588, Japan

Abstract

We report the discovery of the fifth self-lensing binary in which a low-mass white dwarf (WD) gravitationally magnifies its 15th magnitude G-star companion, KIC 8145411, during eclipses. The system was identified from a pair of such self-lensing events in the *Kepler* photometry, and was followed up with the Tillinghast Reflector Echelle Spectrograph (TRES) on the 1.5 m telescope at the Fred Lawrence Whipple Observatory and the High-Dispersion Spectrograph (HDS) on the Subaru 8.2 m telescope. A joint analysis of the TRES radial velocities, the HDS spectrum, and the *Kepler* photometry of the primary star determines the WD mass $0.20 \pm 0.01\,M_\odot$, orbital semimajor axis 1.28 ± 0.03 au, and orbital eccentricity 0.14 ± 0.02. Because such extremely low-mass WDs cannot be formed in isolation within the age of the Galaxy, their formation is believed to involve binary interactions that truncated evolution of the WD progenitor. However, the observed orbit of the KIC 8145411 system is at least 10 times wider than required for this scenario to work. The presence of this system in the *Kepler* sample, along with its similarities to field blue straggler binaries presumably containing WDs, may suggest that some 10% of post-asymptotic giant branch binaries with Sun-like primaries contain such anomalous WDs.

Key words: techniques: photometric – techniques: radial velocities – white dwarfs

1. Introduction

The lowest-mass known white dwarfs (WDs) in the Galaxy have masses below $0.2\,M_\odot$ (e.g., Kilic et al. 2007a). Because the Galaxy is not old enough to produce them through single-star evolution, these so-called extremely low-mass (ELM) WDs with $\lesssim 0.25\,M_\odot$ are considered to be remnants of mass transfer during the red giant branch (RGB) phase, in which the hydrogen envelope of the WD progenitor was stripped to leave a degenerate helium core with $\lesssim 0.45\,M_\odot$, before the star ignites helium and enters the asymptotic giant branch (AGB) phase (e.g., Marsh et al. 1995).

The observations so far appear to be consistent with this scenario. For low-mass WDs identified as companions to millisecond pulsars, the mass transfer model successfully explained the correlation between their orbital periods and WD masses (Rappaport et al. 1995; Tauris & Savonije 1999), as well as the rejuvenated nature of the pulsars. Low-mass WDs have also been identified from the Sloan Digital Sky Survey (SDSS) spectroscopically (Liebert et al. 2004), and the dedicated radial-velocity (RV) companion search (ELM survey; Brown et al. 2010) has found presumably degenerate companions on short-period ($\lesssim$ a few days) orbits for most of

the surveyed WDs with $\lesssim 0.25\,M_\odot$ (Brown et al. 2010; Kilic et al. 2011). Low-mass WDs, or their precursor subdwarf stars, have also been identified as secondary companions to early-type dwarfs on $\lesssim 10$ day orbits via (a combination of) eclipses, relativistic beaming, and ellipsoidal variations in the photometric data both from ground and space (e.g., van Kerkwijk et al. 2010; Maxted et al. 2013; Faigler et al. 2015). The orbital periods and WD masses of these nonpulsar systems are also consistent with RGB mass transfer (see Section 4).

This Letter reports the discovery of an ELM WD eclipsing the stellar companion KIC 8145411 separated by ~ 1 au, which serves as an exception to the above cases. The WD was identified from periodic brightening of KIC 8145411 due to in-eclipse microlensing in the archival photometry of the *Kepler* spacecraft (Borucki et al. 2010). This "self-lensing" has been used to detect four WDs in binaries with orbital periods 88–728 days (Kruse & Agol 2014; Kawahara et al. 2018), and here we report the fifth such case. We characterize the system combining the *Kepler* photometry and ground-based spectroscopy (Section 2), and make a strong case that the companion is an ELM WD even though its light is not observed (Section 3). We discuss the puzzle presented by this system (Section 4), as well as potential evidence that ELM WDs are not rare among post-interaction binaries with au-scale orbits, including so-called field blue straggler (FBS) binaries (Section 5). We also briefly comment on possible formation paths (Section 6).

2. Photometric and Spectroscopic Data

2.1. Kepler *Light Curves*

In Kawahara et al. (2018), we identified KIC 8145411 as a self-lensing binary candidate exhibiting two pulses separated

---

Table 1
TRES Radial Velocities

Time (BJD$_{TDB}$)	Radial Velocity (m s^{-1})	Error (m s^{-1})
2457900.8368	−3575.3	123
2457935.7773	−4867.5	103
2458007.6608	−4657.4	87
2458021.7223	−3667.2	85
2458067.6248	−244.5	67
2458210.9310	2914.0	95
2458256.9529	627.5	87
2458272.9336	0	88
2458292.8412	−1058.1	88
2458390.6203	−5035.2	81
2458419.6013	−5641.4	108
2458439.6326	−4990.9	191

by ≈910 days in the *Kepler* pre-search data conditioning (PDC) light curve. Since the data in the middle of the two pulses were missing, the orbital period was uncertain by a factor of two. We resolve this ambiguity with the RV data presented in this study.

In the following, we mainly use the PDC light curves within ≈2 days around the detected pulses, after iterative detrending with a third-order polynomial function of time as described in Kawahara et al. (2018). We also analyze the simple aperture photometry (SAP) flux to check the robustness of the results against the adopted data set. The cadences are 29.4 minutes in both cases.

2.2. RVs from FLWO/TRES

We obtained 12 high-resolution ($R \sim 44,000$) spectra of KIC 8145411 using the Tillinghast Reflector Echelle Spectrograph (TRES; Szentgyorgyi & Furész 2007; Mink 2011) on the 1.5 m telescope at the Fred Lawrence Whipple Observatory (FLWO) in Arizona. The typical exposure time was ∼1 hr and the signal-to-noise per resolution element was ∼17. The relative RVs were measured by cross-correlating each spectrum against the spectrum with the highest signal-to-noise, as listed in Table 1.

2.3. High-resolution Spectrum from Subaru/HDS

To characterize the primary star, we also obtained a higher signal-to-noise spectrum of KIC 8145411 with the High-Dispersion Spectrograph (HDS; Noguchi et al. 2002) installed on the Subaru 8.2 m telescope. We used the standard I2a setup and the Image Slicer #2 (Tajitsu et al. 2012; $R \sim 80,000$), and obtained one 30 minute exposure. The resulting signal-to-noise was ∼30 per pixel.

3. Physical Model of the System

The new RV data from FLWO/TRES (Section 2.2; Figure 1(a)) confirm that the self-lensing signal in the *Kepler* light curve is due to a companion on a low-eccentricity, 450-day edge-on orbit (Section 3.2). Combined with the primary mass of ≈1.1 $M_{\odot}$ from the Subaru spectrum (Section 3.1, Figure 2), the RV amplitude derives the companion mass of 0.2 $M_{\odot}$. In addition, the self-lensing signal shows that the companion is a compact object smaller than ∼0.02 $R_{\odot}$ (Section 3.3; Figures 1(b)–(c)). Therefore, we have a strong case that the companion is an ELM WD, even though its light is not detected. The upper limit on the WD luminosity placed by the null detection of the secondary

eclipse is consistent with the inferred age of the primary star and the WD cooling model.

3.1. Characterization of the Primary Star

We characterized the visible primary star KIC 8145411 applying the `SpecMatch-Emp` code (Yee et al. 2017) to its high-resolution spectrum (Section 2.3). The stellar parameters are estimated by matching the observed spectrum against a library of high-resolution ($R \approx 60,000$), high signal-to-noise (≈ 150 per pixel) Keck/HIRES spectra of ∼M5–F1 touchtone stars with well-determined physical properties. The input spectrum was resampled and shifted onto the library wavelength scale using cross-correlation, and the best-match library spectra that minimize the sum of squares of the difference were searched by applying a rotational broadening kernel to the library spectra and adjusting $v \sin i$ along with the continuum normalization. Five best-matching library spectra and physical parameters of those stars were identified and linearly interpolated to find the best-match composite spectrum (Figure 2) and the corresponding set of parameters of the target star. The uncertainties of the parameters are estimated based on the accuracy of the parameter recovery when the code is applied to their library stars with known parameters. Since the parallax measurement for KIC 8145411 is not available in the Data Release 2 of *Gaia* (Gaia Collaboration et al. 2018), we simply adopted the outputs of the code, as summarized in the "Spectrum" column in Table 2. Although the covariance between the parameters is not taken into account, that does not affect our analysis because their correlation is dominated by the constraint from self-lensing duration, which scales as $P^{1/3}(M_1/R_1^3)^{-1/3}$ (e.g., Winn 2011).

Considering the importance of the stellar parameter estimation, we also applied the `ZASPE` code (Brahm et al. 2017) to the same Subaru spectrum. We found $T_{\rm eff} = 5751 \pm 96$ K, $\log g = 4.34 \pm 0.20$, [Fe/H] $= 0.36 \pm 0.05$, and $v \sin i = 5.32 \pm 0.25$ km s^{-1}, which are all consistent with the results from `SpecMatch-Emp`.[8] The resulting effective temperature is also consistent with the value (5713^{+154}_{-188} K) in the *Kepler* input catalog (Mathur et al. 2017), which is essentially based on broadband photometry.

3.2. Spectroscopic Orbit

We fitted a Keplerian model to the TRES RV time series (Table 1; Section 2.2) to determine the orbital period P, RV semiamplitude K, eccentricity and argument of periastron referred to the sky $\sqrt{e} \cos \omega$ and $\sqrt{e} \sin \omega$, time of periastron passage τ, radial-velocity zero-point γ, constant acceleration $\dot{\gamma}$, and the RV jitter $\sigma_{\rm RV}$. We used `emcee` (Foreman-Mackey et al. 2013) to sample from the posterior distribution of these parameters via a Markov Chain Monte Carlo algorithm with the affine-invariant ensemble sampler (Goodman & Weare 2010). The log-likelihood function was defined as

$$\ln \mathcal{L} = -\frac{1}{2} \sum_i \frac{(y_i - y_{{\rm model},i})^2}{\sigma_i^2 + \sigma_{\rm RV}^2} - \frac{1}{2} \sum_i \ln(\sigma_i^2 + \sigma_{\rm RV}^2), \quad (1)$$

where y and σ denote the observed RV value and its error, respectively, and $y_{\rm model}$ is the modeled RV value. We adopted

---

[8] Although $v \sin i$ is not included in the outputs of the `SpecMatch-Emp` code, the values used in the five best-match spectra are consistent with the estimate from `ZASPE`.

(a) Radial velocity

(b) First observed pulse

(c) Second observed pulse
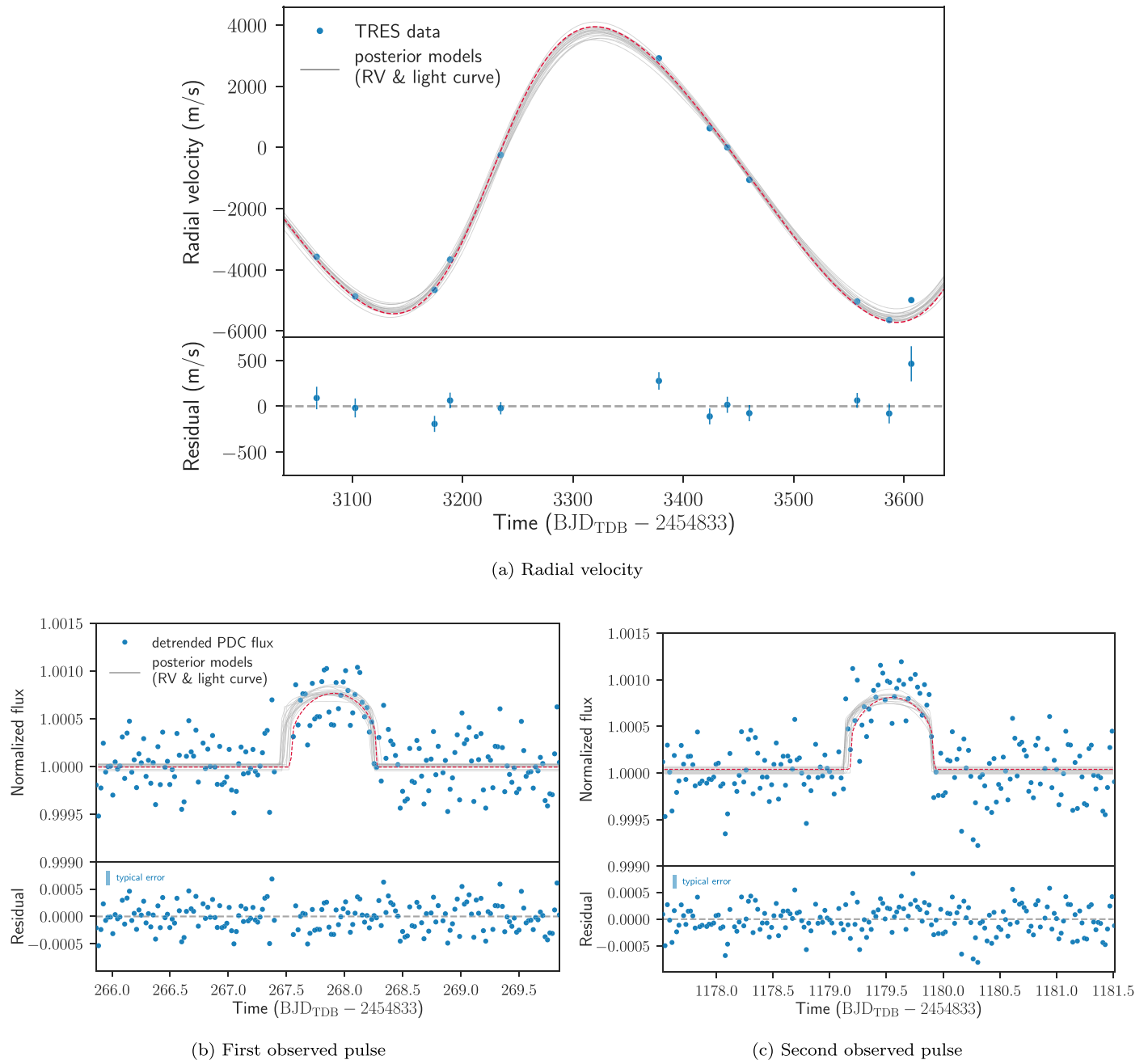
Figure 1. Data (blue points) and 20 random posterior models (gray lines) from the joint analysis in Section 3.3. The red dashed lines show the best-fit model from the analysis assuming the WD mass–radius relation (see Section 3.3). (a) Radial-velocity time series from FLWO/TRES. ((b), (c)) Detrended *Kepler* PDC light curves around self-lensing pulses.

uniform priors for τ, $\sqrt{e}\cos\omega$, $\sqrt{e}\sin\omega$, γ, and $\dot{\gamma}$; and loguniform ones for P, K, and σ_{RV}.

The resulting constraints are summarized in the "RV" column in Table 2. The orbital period turned out to be half the interval of the two detected self-lensing pulses, meaning that one pulse was missed in the data gap. The binary mass function $(4.8 \pm 0.4) \times 10^{-3}\, M_\odot$, combined with the primary mass $1.12 \pm 0.08\, M_\odot$ (Section 3.1) and the orbital inclination $\approx 90°$ (as justified from self-lensing signals), yields the WD mass of $0.20 \pm 0.01\, M_\odot$. We also find the orbital semimajor axis of 1.26 ± 0.03 au and eccentricity of 0.14 ± 0.02.

We did not find strong evidence for radial acceleration $\dot{\gamma}$ due to a tertiary companion. The current limit $|\dot{\gamma}| \lesssim 1\ \mathrm{m\ s^{-1}\ day^{-1}}$

implies $m_3 \sin i_3 / a_3^2 \lesssim M_\odot / (20\ \mathrm{au})^2$ for the mass m_3, orbital inclination i_3, and semimajor axis a_3 of the potential tertiary companion.

3.3. Combined Analysis

To check that the RV time series and the *Kepler* self-lensing light curves are consistently explained, we jointly modeled the two data sets incorporating the knowledge of the primary star from spectroscopy. We defined the likelihood function for the photometric data in a similar way to Equation (1), where the additional white-noise term (photometric jitter) was introduced analogously to σ_{RV}. Here we adopted independent photometric
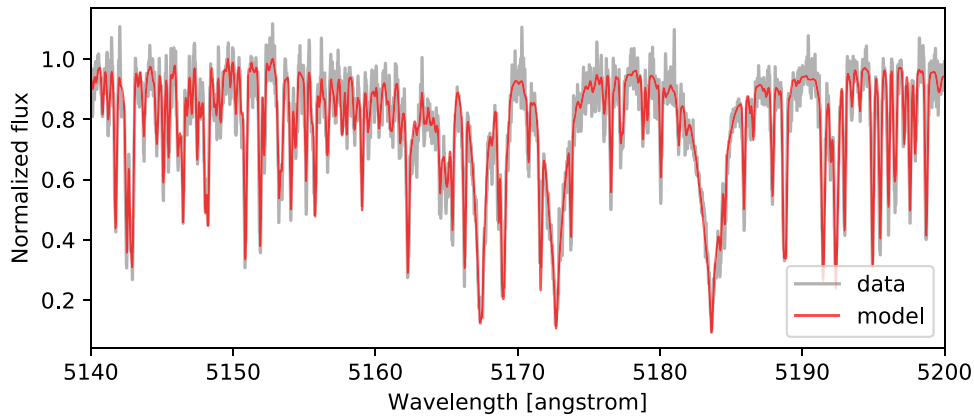
Figure 2. A portion of the HDS spectrum of the primary star (gray) and the best-match model from `SpecMatch-Emp` (red).

jitters for the first and second pulses because the *Kepler* data around the second pulse were obtained during reaction-wheel zero crossings and the raw SAP light curve shows some artificial dips that have been corrected in the PDC pipeline (Smith et al. 2012; Stumpe et al. 2012). The correction could introduce systematics that affect the noise level, and the two jitter terms are introduced to account for this possibility. The self-lensing light curves were modeled mostly in the same way as in Kawahara et al. (2018): the light curve was computed as the sum of the WD eclipse and self-lensing pulse, where the latter was approximated as an inverted eclipse whose height is determined by the Einstein radius of the WD instead of its physical radius (Agol 2003). The normal/inverted eclipse light curves were computed using the Mandel & Agol (2002) model for the quadratic limb-darkening law as implemented in `PyTransit` (Parviainen 2015), where the limb-darkening coefficients (u_1, u_2) were parameterized following Kipping (2013). Here we chose the WD radius to be a free parameter rather than a deterministic function of the WD mass: given that the amplitude of the self-lensing pulse is fixed through the WD mass from RVs, the WD radius can be constrained from the eclipse component (see, e.g., Yahalomi et al. 2019).

The results are summarized in Table 2 and the posterior models are shown in Figure 1 with gray lines. The RVs and light curves are consistently modeled, and the resulting constraints are mostly unchanged from the RV-only model except that the orbital period is more precisely determined. The main results including the WD mass are mostly insensitive to which of the PDC and SAP light curves is adopted. We confirmed the compact nature of the companion, placing upper limits on its radius, $<0.022\,R_\odot$ from the SAP data and $<0.015\,R_\odot$ from the PDC data, which are independent from the WD model.

The zero-temperature WD model predicts $\approx 0.02\,R_\odot$ for the measured mass of $0.2\,M_\odot$ (Nauenberg 1972; see also Figure 13 of Kawahara et al. 2018), which is formally inconsistent with the PDC value and barely consistent with the SAP one. Although these limits, if taken at face value, are potentially interesting, we note that the quantitative constraint on this parameter depends on subtle eclipse signals of order 10^{-4} and would be of limited reliability given the quality issue of the light curve discussed above. Indeed, comparing the data and models in Figures 1(b) and (c), the second pulse appears to be slightly higher; this suggests that unmodeled systematics exist in the data, which may also be the origin of different limits obtained from SAP and PDC data. Thus, at the moment we do not consider this limit to be sufficiently strong evidence for more exotic explanations including a black hole and a neutron star, although the current data, including the absence of secondary eclipses as discussed below, are compatible with such scenarios as well. Follow-up observations of more self-lensing events with a precision comparable to or better than *Kepler* would be required to resolve this issue. To make sure that this possible tension does not significantly affect the measured WD mass, we also repeated the same analysis for the PDC data imposing the Eggleton mass–radius relation (Verbunt & Rappaport 1988) for the companion. We found $0.22 \pm 0.01\,M_\odot$ for the WD mass, which is only marginally different from the above result. The best-fit model from this analysis is shown with red dashed lines in Figure 1. The small difference from the previous analysis (gray lines) highlights the subtlety involved in measuring the WD radius accurately.

The impact parameter during self-lensing events, along with e and ω, indicates that the WD was totally occulted by the primary. Nevertheless, we did not clearly detect secondary eclipses at the expected times. To check if this is consistent with the WD interpretation, we performed another analysis including the PDC data around the expected secondary eclipse times and imposing the Eggleton mass–radius relation. Here the WD effective temperature $T_{\rm WD}$ is an additional free parameter constrained from the absence of secondary eclipses, whose depth in the model was computed by convolving the blackbody spectra of the WD and the primary star with the response function of *Kepler*. The effective temperature of the primary was fixed to be 5724 K from spectroscopy. The posterior models around expected secondary eclipse times from this analysis are compared with the data in Figure 3. The lack of clear secondary eclipses requires $T_{\rm WD} \lesssim 5000$ K (95% limit), which is consistent with theoretical evolutionary models of WDs older than a few Gyr (Figure 4). This is also compatible with the crude spectroscopic age of the primary star $6.5^{+3.1}_{-2.1}$ Gyr, although the value is not very well constrained and may need to be interpreted with care if the system has experienced mass transfer in the past. Considering that the system has been identified via self-lensing, it is not very unnatural that the detected WD has cooled down because self-lensing signals are diminished for younger low-mass WDs with larger physical radii.

4

Table 2
Parameters of the KIC 8145411 System

|	Spectrum	RV	RV and *Kepler* SAP	RV and *Kepler* PDC
(*Orbital Parameters*)				
time of periastron passage τ (BJD$_{\mathrm{TDB}}$ − 2,454,833)	⋯	3233^{+11}_{-12}	$488.6^{+3.7}_{-6.5}$	$489.6^{+3.1}_{-4.5}$
period P (days)	⋯	$448.6^{+5.8}_{-5.2}$	$455.870^{+0.015}_{-0.015}$	$455.826^{+0.009}_{-0.011}$
$\sqrt{e}\cos\omega$	⋯	$0.019^{+0.063}_{-0.066}$	$-0.024^{+0.018}_{-0.016}$	$-0.022^{+0.014}_{-0.014}$
$\sqrt{e}\sin\omega$	⋯	$-0.364^{+0.028}_{-0.021}$	$-0.363^{+0.030}_{-0.021}$	$-0.378^{+0.017}_{-0.019}$
RV semiamplitude K (km s^{-1})	⋯	$4.73^{+0.14}_{-0.13}$	$4.579^{+0.083}_{-0.102}$	$4.623^{+0.077}_{-0.075}$
RV zero-point γ (m s^{-1})	⋯	-687^{+75}_{-74}	-748^{+65}_{-68}	-726^{+62}_{-58}
constant acceleration $\dot{\gamma}$ (m s^{-1} day^{-1})	⋯	$-0.33^{+0.31}_{-0.32}$	$-0.52^{+0.32}_{-0.30}$	$-0.51^{+0.31}_{-0.28}$
semimajor axis a (au)	⋯	$1.254^{+0.031}_{-0.031}$[a]	$1.270^{+0.027}_{-0.028}$	$1.276^{+0.027}_{-0.028}$
eccentricity e	⋯	0.135 ± 0.018	$0.132^{+0.016}_{-0.021}$	$0.143^{+0.015}_{-0.012}$
argument of periastron ω (degrees)	⋯	$-86.9^{+9.6}_{-10.7}$	$-93.7^{+2.8}_{-2.5}$	$-93.4^{+2.1}_{-2.2}$
inclination i (degrees)	⋯	⋯	$89.929^{+0.046}_{-0.035}$	$89.976^{+0.017}_{-0.025}$
periastron distance $a(1-e)$ (au)	⋯	$1.084^{+0.033}_{-0.033}$[a]	$1.102^{+0.036}_{-0.033}$	$1.091^{+0.031}_{-0.032}$
mass function ($M_\odot$)	⋯	$4.77^{+0.42}_{-0.38} \times 10^{-3}$	$4.41^{+0.24}_{-0.27} \times 10^{-3}$	$4.52^{+0.22}_{-0.21} \times 10^{-3}$
(*Primary Parameters*)				
mass M_1 ($M_\odot$)	1.11 ± 0.08	⋯	$1.118^{+0.079}_{-0.077}$	$1.132^{+0.078}_{-0.078}$
radius R_1 ($R_\odot$)	1.27 ± 0.18	⋯	$1.195^{+0.082}_{-0.084}$	$1.269^{+0.045}_{-0.047}$
effective temperature T_{eff} (K)	5724 ± 110	⋯	⋯	⋯
surface gravity $\log_{10}(\mathrm{g/cm\ s^{-2}})$	4.20 ± 0.12	⋯	⋯	⋯
metallicity [Fe/H]	0.39 ± 0.09	⋯	⋯	⋯
age $\log_{10}(\mathrm{age\ yr^{-1}})$	9.81 ± 0.17	⋯	⋯	⋯
(*White-dwarf Parameters*)				
mass M_2 ($M_\odot$)	⋯	$0.201^{+0.012}_{-0.011}$[a]	$0.197^{+0.010}_{-0.010}$	$0.200^{+0.009}_{-0.009}$
radius R_2 ($R_\odot$)	⋯	⋯	<0.022 (99.7% limit)	<0.015 (99.7% limit)
(*Light-curve Parameters*)				
time of inferior conjunction $t_{0,\mathrm{pulse}}$ (BJD$_{\mathrm{TDB}}$ − 2,454,833)	⋯	313^{+37}_{-41}	$267.895^{+0.016}_{-0.017}$	$267.867^{+0.022}_{-0.017}$
time of superior conjunction $t_{0,\mathrm{secondary}}$ (BJD$_{\mathrm{TDB}}$ − 2,454,833)	⋯	539^{+31}_{-34}	$493.3^{+1.9}_{-1.7}$	$493.4^{+1.5}_{-1.6}$
impact parameter (primary eclipse) b_{pulse}	⋯	⋯	$0.32^{+0.15}_{-0.20}$	$0.10^{+0.11}_{-0.07}$
impact parameter (secondary eclipse) $b_{\mathrm{secondary}}$	⋯	⋯	$0.25^{+0.11}_{-0.16}$	$0.078^{+0.079}_{-0.055}$
limb-darkening coefficient $q_1 = (u_1 + u_2)^2$	⋯	⋯	$0.68^{+0.23}_{-0.30}$	$0.38^{+0.34}_{-0.23}$
limb-darkening coefficient $q_2 = u_1/2(u_1 + u_2)$	⋯	⋯	$0.54^{+0.29}_{-0.32}$	$0.37^{+0.35}_{-0.25}$
flux normalization (1st pulse) c_1	⋯	⋯	$1.000001^{+0.000020}_{-0.000020}$	$1.000004^{+0.000021}_{-0.000020}$
flux normalization (2nd pulse) c_2	⋯	⋯	$1.000033^{+0.000026}_{-0.000026}$	$1.000023^{+0.000020}_{-0.000020}$
(*Jitters*)				
RV jitter $\log_{10}\sigma_{\mathrm{RV}}$ (m s^{-1})	⋯	$1.95^{+0.32}_{-1.02}$	$2.13^{+0.22}_{-0.40}$	$2.06^{+0.24}_{-0.55}$
photometric jitter (1st pulse) $\log_{10}\sigma_1$	⋯	⋯	<-3.9 (99.7% limit)	<-3.9 (99.7% limit)
photometric jitter (2nd pulse) $\log_{10}\sigma_2$	⋯	⋯	$-3.672^{+0.058}_{-0.069}$	<-3.8 (99.7% limit)

Notes. The values are the medians and symmetric 68.3% regions of the marginal posteriors.
[a] These values are derived assuming $i = 90°$ and the primary mass from spectroscopy.

4. "Impossible" ELM WD?

The orbit of the KIC 8145411 system is far wider than known binaries containing ELM WDs and challenges the standard formation scenario through RGB mass transfer. To produce such a WD, the envelope of the WD progenitor needs to be stripped when its core had ≈0.2 $M_\odot$ in the RGB phase. The radius of such an RGB star never exceeds 9 $R_\odot \approx 0.04$ au, which we confirmed using the MESA code (Paxton et al. 2011, 2013, 2015, 2018), and the orbit needs to be comparably tight for the binary to interact. Indeed, known binaries with ELM WDs have such tight orbits as shown in Figure 5, where

we plot the WDs in binaries and with measured masses collected from the literature. The gray line quantifies the above argument about the relation between the orbit and the WD mass with numerical calculations for the stable mass transfer case (Lin et al. 2011): this well matches the upper envelope of the known systems, regardless of the WD mass and type of companions. Thus, they are compatible with formation through stable mass transfer, or common-envelope evolution in which the orbit shrank due to dynamical friction (Paczynski 1976). However, the KIC 8145411 system has a much wider orbit than predicted from this relation, and it should have been impossible
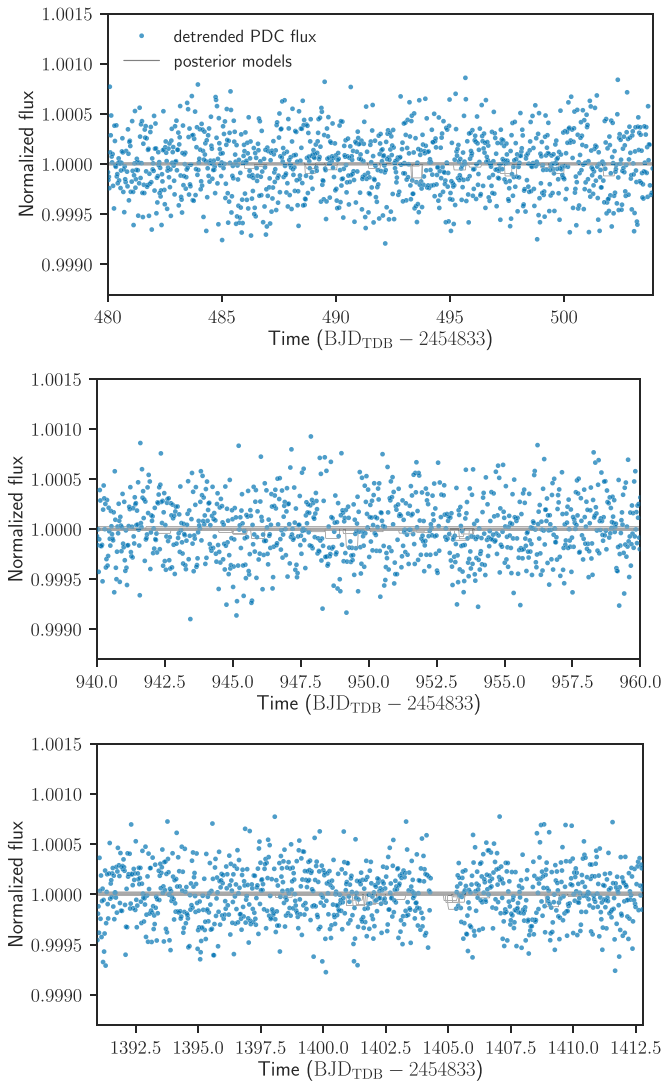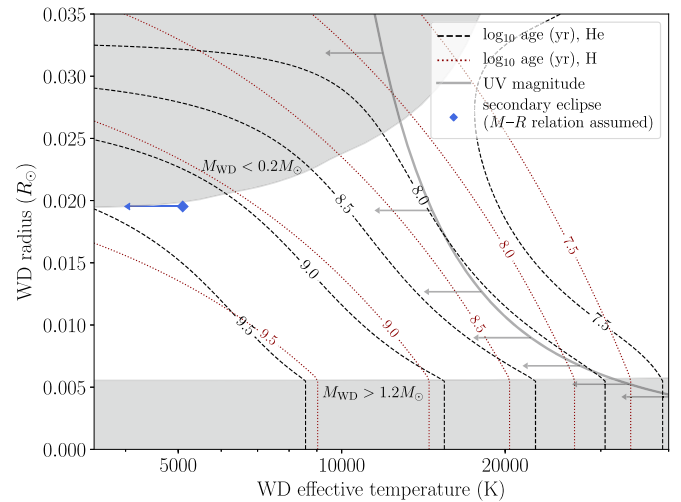
Figure 3. Detrended PDC light curves around the expected times of secondary eclipses (blue points) and 20 random posterior models (gray lines) from the joint analysis of RVs, self-lensing pulses, and the data shown in this plot (Section 3.3). Here the WD radius is related to its mass via a physical mass–radius relation, and the effective temperature of the WD is an additional free parameter.


Figure 4. Constraints on the WD radius and effective temperature based on the absence of secondary eclipses and physical mass–radius relation (blue diamond), compared with evolutionary models for hydrogen (red dotted) and helium (black dashed) atmosphere WDs from http://www.astro.umontreal.ca/~bergeron/CoolingModels (Holberg & Bergeron 2006; Kowalski & Saumon 2006; Bergeron et al. 2011; Tremblay et al. 2011). The models are not available for the gray shaded regions. The gray solid line shows the constraint from the absence of UV excess in the *GALEX* data; see Section 3.3 of Kawahara et al. (2018) for details.

for the progenitor of the WD, when its core was $\approx0.2\,M_\odot$, to have filled its Roche lobe. Considering that the progenitor was initially more massive, the Roche-lobe radius around the progenitor was $\gtrsim0.5$ au for $a = 1.28$ au, which is >10 times larger than the radius of the progenitor.

We do not have a definitive solution to this puzzle, and there appears to be something missing in our understanding of the formation of ELM WDs and/or binary interactions. In the following sections, we discuss observational implications of this finding, and briefly comment on possible formation paths.

4.1. Could the Primary Mass Be Incorrect?

Could the anomalous WD mass be due to misclassification of the primary star? One might be worried that some peculiar evolutionary history of the system (e.g., significant mass transfer) could affect the interpretation of the spectrum. While we believe that parameters such as $T_{\rm eff}$, $\log g$, and [Fe/H] are unaffected because they are only based on model stellar atmospheres, it may still be possible that the relation between the atmospheric parameters and bulk stellar properties is systematically biased because they are tied using evolutionary models of a single isolated star.

Given the difficulty of modifying stellar models accordingly, here we ask the following question: how wrong do the primary mass and radius need to be for the companion WD to be a "normal" one? Figure 6 shows the relation between the secondary and primary masses for the binary mass function $4.8 \times 10^{-3}\,M_\odot$ *measured* from the RV data. The thick solid gray line shows that the primary mass of $\approx1.1\,M_\odot$ corresponds to the companion mass of $\approx0.2\,M_\odot$, as we presented. The thick dashed line shows that, if the companion has $\approx0.4\,M_\odot$ as theoretically expected from the observed binary period (see the gray line in Figure 5), the primary has to have $\approx3.3\,M_\odot$ to reproduce the observed RV amplitude. On the other hand, this change should also affect the amplitude of the self-lensing signal, which scales as $M_{\rm WD}/R_1^2$; thus, R_1 also needs to be $\sqrt{2}$ times larger than the current estimate and should be $\sim1.8\,R_\odot$ to produce the same self-lensing signal for $M_{\rm WD} = 0.4\,M_\odot$. Therefore, the current RV and self-lensing data allow the WD companion to have the theoretically expected mass and orbital period only if the primary is a B- or A-type main-sequence star. This case is excluded from the spectrum presented in Section 3.1 and Figure 2.

5. Occurrence Rate of Similar Systems and Connections to FBS Binaries

The eclipse probability of the KIC 8145411 system is $R_1/a(1 - e^2) \approx 1/200$, while it was found among $\sim10^5$ *Kepler* stars showing sufficiently small photometric noise. Thus, such ELM WD companions should occur around $\sim200/10^5 = 0.2\%$ of Sun-like stars, and the actual rate could be higher if the search incompleteness is corrected. On the other hand, the occurrence rate of WD companions with au-scale orbits around Sun-like stars, regardless of the WD mass, is likely a few percent (e.g., Moe & Di Stefano 2017; Murphy et al. 2018). Their ratio implies
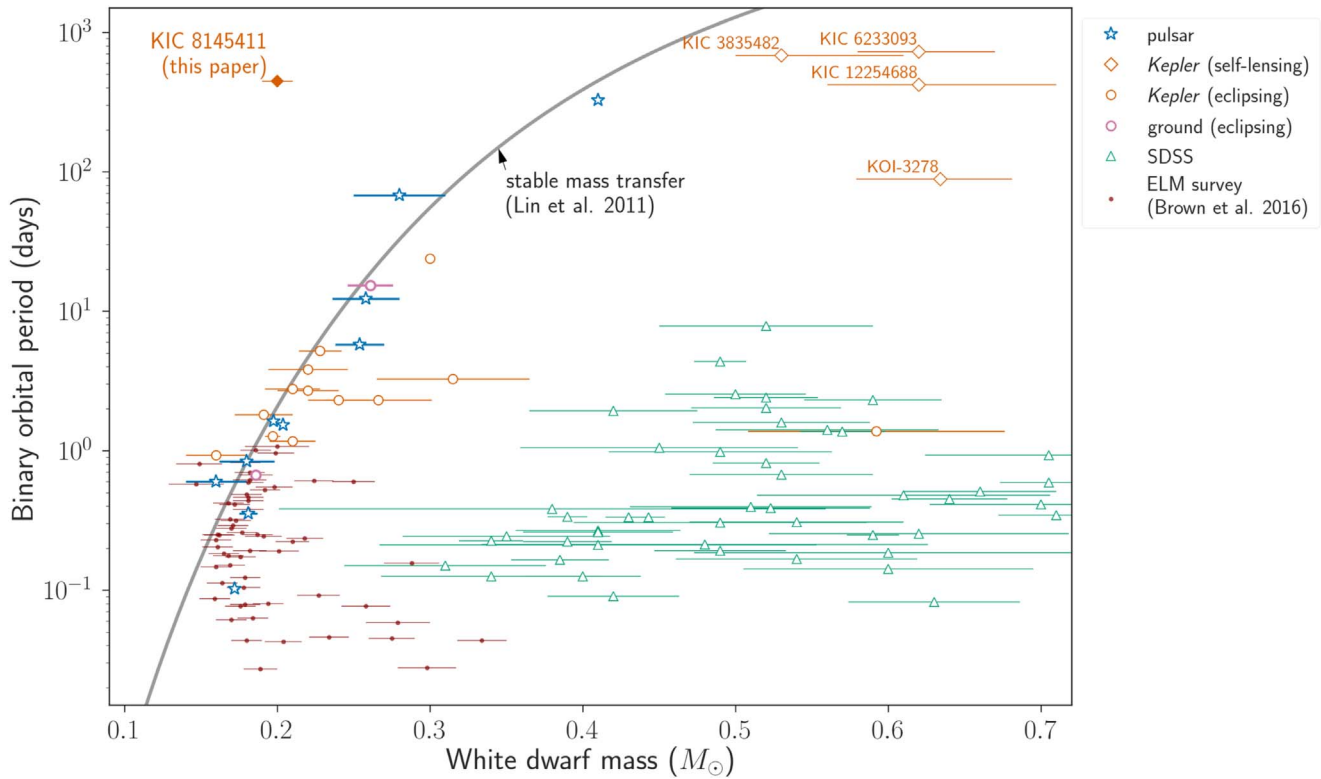
Figure 5. Masses of WDs in binaries and their orbital periods. The KIC 8145411 system (upper left) and other self-lensing systems (Kruse & Agol 2014; Kawahara et al. 2018) are shown with orange diamonds. The gray line is the theoretical P–M_{WD} relation for the stable mass transfer case by Lin et al. (2011). Blue stars denote the systems with pulsar companions compiled by Tauris & van den Heuvel (2014); orange and pink circles are those eclipsing stellar companions from *Kepler* (van Kerkwijk et al. 2010; Carter et al. 2011; Breton et al. 2012; Muirhead et al. 2013; Faigler et al. 2015; Rappaport et al. 2015; Zhang et al. 2017) and ground-based data (OGLE and WASP surveys; Pietrzyński et al. 2012; Maxted et al. 2013), respectively; green triangles are WD–main-sequence binaries from the SDSS (Rebassa-Mansergas et al. 2012); filled maroon circles are from the ELM survey (Brown et al. 2016).
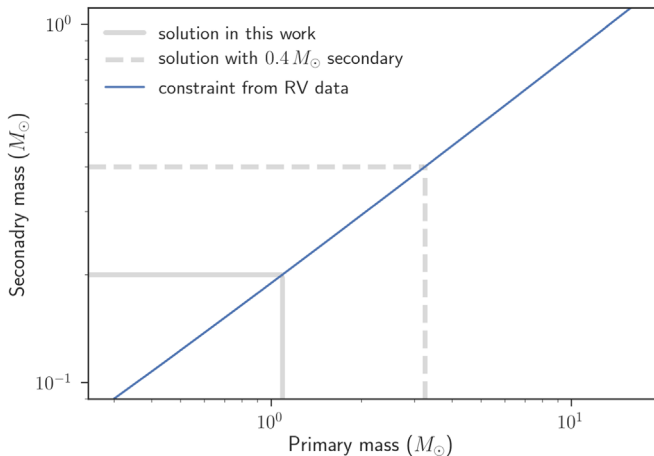
Figure 6. Secondary and primary masses from the RV data. The blue solid line shows their relation based on the observed binary mass function of $4.8 \times 10^{-3} M_\odot$. The thick solid and dashed gray lines show the solution found in this work (i.e., $0.2 M_\odot$ companion) and that with a $0.4 M_\odot$ companion as theoretically expected from the binary orbital period (gray line in Figure 5; see also Section 4), respectively.

that $f_{ELM} = 0.2\%$/a few $\% \sim 10\%$ of WD companions of Sun-like stars on au-scale orbits are ELM WDs. The estimate is also consistent, in the order-of-magnitude sense, with the fact that KIC 8145411 is one of four self-lensing WD binaries (i.e., $f_{ELM} = 25\%$) with similar periods identified in Kawahara et al. (2018).

While the above f_{ELM} estimated from single detection is highly uncertain, the value may also be supported by a larger population of FBS binaries as studied in Preston & Sneden (2000) and Carney et al. (2001, 2005), which carry many similarities to the KIC 8145411 system and other self-lensing WD binaries in Kawahara et al. (2018). Their primaries are old halo/thick-disk stars that appear to be too blue given their ages and represent field analogs of blue stragglers in clusters. Their higher binary fraction, smaller companions masses, and lower eccentricities compared to normal binaries; absence of the companion's spectral features; and rapid rotation of the primary all suggest that a majority of these FBSs, if not all, are products of mass transfer (McCrea 1964) and that the unseen companions are WDs. Figure 7 compares these FBS binaries with self-lensing systems: the FBS sample is essentially the same as in Figure 10 of Carney et al. (2005), but here we computed the companion masses of CS 29497–030 and CS 29509–027 (not in Table 5 of their paper) using the RV solution in Sneden et al. (2003) and the primary masses derived by fitting (Morton 2015) the Dartmouth isochrones (Dotter et al. 2008) to the atmospheric parameters in Roederer et al. (2014), the parallax from *Gaia* DR2 (Gaia Collaboration et al. 2018), and the K-magnitude from the Two Micron All Sky Survey (2MASS; Skrutskie et al. 2006). Interestingly, some of the FBS companions are located close to KIC 8145411, 7 out of 19 having minimum masses $<0.25 M_\odot$. For random orbital inclinations, this implies that effectively 4.6 would have *true* masses $<0.25 M_\odot$ (i.e., $f_{ELM} \approx 20\%$).
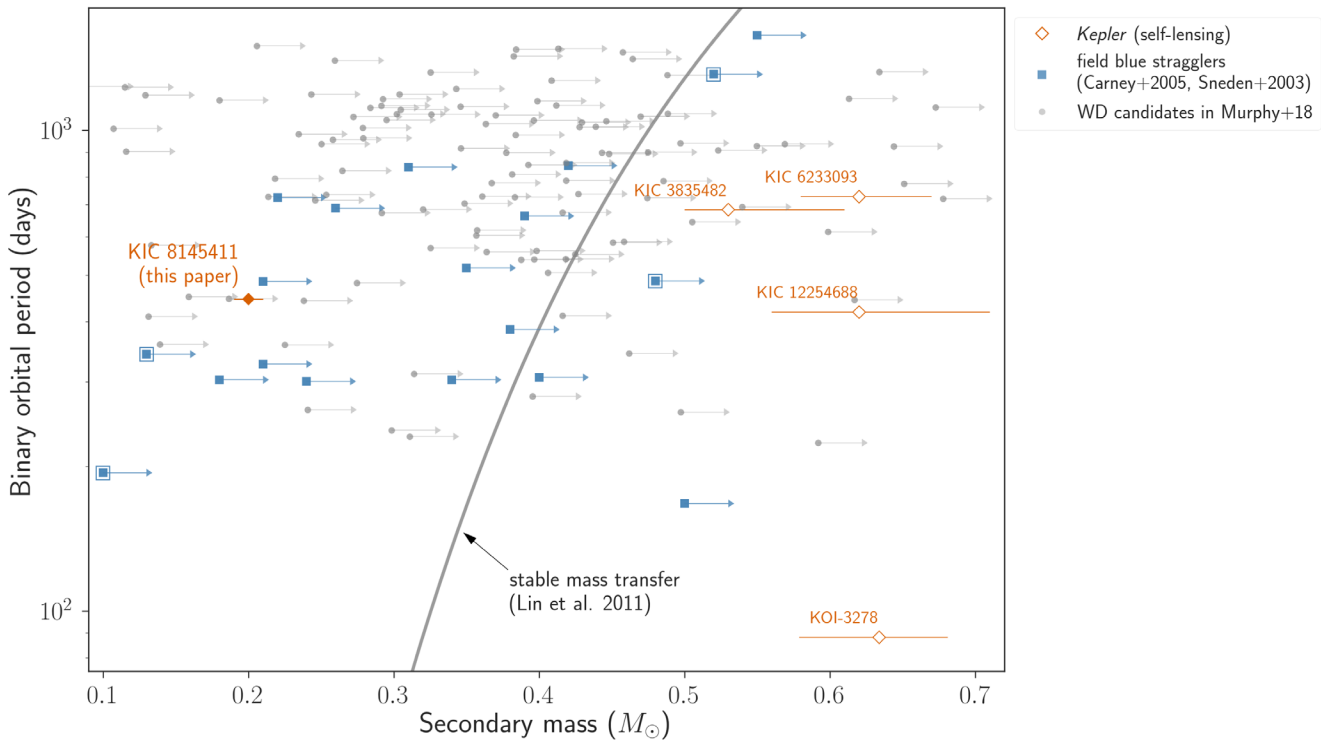
Figure 7. Same as Figure 5, but for WD candidates in stellar binaries with $P \gtrsim 80$ days. Here the minimum masses of the companions in FBS binaries (Sneden et al. 2003; Carney et al. 2005) are shown by blue squares with arrows; those with outer squares are the systems with enhancements of neutron-capture elements detected (Preston & Sneden 2000; Sneden et al. 2003). Gray circles with arrows are the minimum masses of WD candidates identified in Murphy et al. (2018): ≈40% of them are estimated to be WDs, although the identities of individual companions are unclear (see Section 5).

Murphy et al. (2018) also identified similar systems with A/F-type primaries showing δ-Scuti pulsations in the *Kepler* light curves. Analyzing pulsation-phase modulations caused by light-travel time effect, they identified noneclipsing, unseen companions to these stars that contain an excess population of near-circular, au-scale binaries. Murphy et al. (2018) argued that the companions in ≈40% of these ≈120 near-circular systems, defined by the relation $e < 0.55 \log(P/\mathrm{day}) - 1.21$ based on post-AGB binaries, are likely WDs. These near-circular systems are plotted with gray circles in Figure 7, where the minimum secondary masses are computed assuming primary masses in the *Kepler* input catalog (Mathur et al. 2017). If the sample indeed contains WDs and they have the same mass distribution as the whole sample, the minimum-mass distribution of the sample implies $f_{\mathrm{ELM}} \approx 10\%$ for random orbital inclinations.

To summarize, in light of the detection in the KIC 8145411 system, it appears possible that some of the low-mass companions in the above two families of FBS binaries are also ELM WDs. If most of them are so, they imply $f_{\mathrm{ELM}} \approx 10\%-20\%$, which supports the value inferred from the KIC 8145411 system alone.

This conjecture does not contradict the finding of the ELM survey that most of the surveyed ELM WDs were found to be in tight degenerate binaries (e.g., Brown et al. 2010), because they are parts of the SDSS WDs, which do not include WDs with much brighter stellar companions like KIC 8145411. Rather, systems like KIC 8145411 could be progenitors of the ELM WDs in tight degenerate binaries: the mass transfer from the more massive, current stellar primary will likely be unstable, and the system may undergo common-envelope evolution to form a tight binary consisting of an ELM WD and a more massive WD.

6. Summary and Discussion

We confirmed the fifth self-lensing binary consisting of a $0.2\,M_\odot$ WD and a G-type star KIC 8145411. The WD mass measured from RVs and self-lensing events is anomalously low given its au-scale orbit, which is far wider than required for the binary to have interacted to produce such a low-mass WD. Because only 1 in 200 such systems has edge-on geometry to show self-lensing, this system likely represents only the tip of the iceberg. More such low-mass WDs in noneclipsing binaries may be identified with *Gaia* astrometry and/or RV searches combined with complementary observations to show that the companion is too faint to be a star (e.g., Kane et al. 2019), providing a more complete view of post-interaction binaries with WDs and possibly the solution of the puzzle. Below we briefly comment on possible modifications to the standard binary evolution path to explain such anomalous systems, which all appear to involve some difficulties.

There may exist a path involving a tertiary star that made it possible for the binary to interact when the WD progenitor was in the RGB phase. For example, the orbit may have once been highly eccentric due to perturbations from the tertiary star, or may have been significantly widened via a rare stellar encounter after the binary interaction in a close-in orbit. However, it may be difficult for these scenarios to explain why the resulting orbit is nearly circular and why ELM WDs do not appear to be very rare among au-scale WD binaries, as argued in Section 5.

Scenarios that do not involve currently detectable companions have also been proposed. Nelemans & Tauris (1998) proposed that the envelope of the WD progenitor could be stripped by a massive planet or a brown dwarf, which may then

be merged with the resulting WD or evaporate to leave a single low-mass WD. Kilic et al. (2007b) argued that strong wind mass loss from metal-rich stars could truncate the AGB phase to produce single low-mass WDs. Although our system alone does not fully exclude these scenarios, they appear to be unsatisfactory because the low-eccentricity orbit of KIC 8145411, as well as those of the FBS binaries with ELM WDs (if they indeed are), suggest that generally the WD progenitors did interact with the observed stellar primaries.

Alternatively, the WD progenitor might indeed have become large enough (e.g., an AGB star) for the binary to interact in the current ~ 1 au orbit. In this case, the core mass should have already been substantially larger than the current WD mass, as illustrated by the gray line in Figures 5 and 7, and the core somehow needs to lose $\sim 50\%$ of its mass during or after the interaction. While we are not aware of such a mechanism, it is interesting to note that enhancements of carbon and neutron-capture elements have been detected in some of the FBS systems including those with the smallest minimum-mass companions (double squares in Figure 7; Sneden et al. 2003), providing evidence for AGB mass transfer. Future measurements of true masses for these FBS companions with orbital inclinations from *Gaia* would further test this hypothesis.

Note added in proof. In the process of publishing this Letter we learned of a recent study by Vos et al. (2018), who identified an ELM pre-WD (mass $0.23 \pm 0.05\ M_\odot$, effective temperature $26{,}200 \pm 1{,}500$ K, and log surface gravity 5.40 ± 0.35) in a 771-day period, near-circular orbit around a K-dwarf star. The hot primary HE 0430–2457 will evolve into a WD and occupy a similar region of the parameter space as the KIC 8145411 system in Figure 5. Vos et al. (2018) proposed a formation path similar to the one by Nelemans & Tauris (1998) discussed above, that the observed ELM pre-WD is a merger product of a tight binary that has lost a significant fraction of its mass, and that the current stellar companion was initially a tertiary star that did not directly interact with the pre-WD. However, this scenario still seems unable to explain why the current orbit

of the HE 0430–2457 system (as well as KIC 8145411) is nearly circular, as we discussed in Section 6.

ORCID iDs

Kento Masuda https://orcid.org/0000-0003-1298-9699
Hajime Kawahara https://orcid.org/0000-0003-3309-9134
David W. Latham https://orcid.org/0000-0001-9911-7388
Allyson Bieryla https://orcid.org/0000-0001-6637-5401
Morgan MacLeod https://orcid.org/0000-0002-1417-8024
Wako Aoki https://orcid.org/0000-0002-8975-6829

References

Agol, E. 2003, ApJ, 594, 449
Bergeron, P., Wesemael, F., Dufour, P., et al. 2011, ApJ, 737, 28
Borucki, W. J., Koch, D., Basri, G., et al. 2010, Sci, 327, 977
Brahm, R., Jordán, A., Hartman, J., & Bakos, G. 2017, MNRAS, 467, 971
Breton, R. P., Rappaport, S. A., van Kerkwijk, M. H., & Carter, J. A. 2012, ApJ, 748, 115
Brown, W. R., Gianninas, A., Kilic, M., Kenyon, S. J., & Allende Prieto, C. 2016, ApJ, 818, 155
Brown, W. R., Kilic, M., Allende Prieto, C., & Kenyon, S. J. 2010, ApJ, 723, 1072
Carney, B. W., Latham, D. W., & Laird, J. B. 2005, AJ, 129, 466
Carney, B. W., Latham, D. W., Laird, J. B., Grant, C. E., & Morse, J. A. 2001, AJ, 122, 3419
Carter, J. A., Rappaport, S., & Fabrycky, D. 2011, ApJ, 728, 139
Dotter, A., Chaboyer, B., Jevremović, D., et al. 2008, ApJS, 178, 89
Faigler, S., Kull, I., Mazeh, T., et al. 2015, ApJ, 815, 26
Foreman-Mackey, D., Hogg, D. W., Lang, D., & Goodman, J. 2013, PASP, 125, 306
Gaia Collaboration, Brown, A. G. A., Vallenari, A., et al. 2018, A&A, 616, A1
Goodman, J., & Weare, J. 2010, Communications in Applied Mathematics and Computational Science, 5, 65
Holberg, J. B., & Bergeron, P. 2006, AJ, 132, 1221
Kane, S. R., Dalba, P. A., Horner, J., et al. 2019, ApJ, 875, 74
Kawahara, H., Masuda, K., MacLeod, M., et al. 2018, AJ, 155, 144
Kilic, M., Allende Prieto, C., Brown, W. R., & Koester, D. 2007a, ApJ, 660, 1451
Kilic, M., Brown, W. R., Allende Prieto, C., et al. 2011, ApJ, 727, 3
Kilic, M., Stanek, K. Z., & Pinsonneault, M. H. 2007b, ApJ, 671, 761
Kipping, D. M. 2013, MNRAS, 435, 2152
Kowalski, P. M., & Saumon, D. 2006, ApJL, 651, L137
Kruse, E., & Agol, E. 2014, Sci, 344, 275
Liebert, J., Bergeron, P., Eisenstein, D., et al. 2004, ApJL, 606, L147
Lin, J., Rappaport, S., Podsiadlowski, P., et al. 2011, ApJ, 732, 70
Mandel, K., & Agol, E. 2002, ApJL, 580, L171
Marsh, T. R., Dhillon, V. S., & Duck, S. R. 1995, MNRAS, 275, 828
Mathur, S., Huber, D., Batalha, N. M., et al. 2017, ApJS, 229, 30
Maxted, P. F. L., Serenelli, A. M., Miglio, A., et al. 2013, Natur, 498, 463
McCrea, W. H. 1964, MNRAS, 128, 147
Mink, D. J. 2011, in ASP Conf. Ser. 442, Astronomical Data Analysis Software and Systems XX, ed. I. N. Evans et al. (San Francisco, CA: ASP), 305
Moe, M., & Di Stefano, R. 2017, ApJS, 230, 15
Morton, T. D. 2015, isochrones: Stellar Model Grid Package, Astrophysics Source Code Library, ascl:1503.010
Muirhead, P. S., Vanderburg, A., Shporer, A., et al. 2013, ApJ, 767, 111
Murphy, S. J., Moe, M., Kurtz, D. W., et al. 2018, MNRAS, 474, 4322
Nauenberg, M. 1972, ApJ, 175, 417
Nelemans, G., & Tauris, T. M. 1998, A&A, 335, L85
Noguchi, K., Aoki, W., Kawanomoto, S., et al. 2002, PASJ, 54, 855
Paczynski, B. 1976, in IAU Symp. 73, Structure and Evolution of Close Binary Systems, ed. P. Eggleton, S. Mitton, & J. Whelan (Dordrecht: Reidel), 75
Parviainen, H. 2015, MNRAS, 450, 3233
Paxton, B., Bildsten, L., Dotter, A., et al. 2011, ApJS, 192, 3
Paxton, B., Cantiello, M., Arras, P., et al. 2013, ApJS, 208, 4
Paxton, B., Marchant, P., Schwab, J., et al. 2015, ApJS, 220, 15
Paxton, B., Schwab, J., Bauer, E. B., et al. 2018, ApJS, 234, 34
Pietrzyński, G., Thompson, I. B., Gieren, W., et al. 2012, Natur, 484, 75
Preston, G. W., & Sneden, C. 2000, AJ, 120, 1014
Rappaport, S., Nelson, L., Levine, A., et al. 2015, ApJ, 803, 82

Rappaport, S., Podsiadlowski, P., Joss, P. C., Di Stefano, R., & Han, Z. 1995, MNRAS, 273, 731

Rebassa-Mansergas, A., Nebot Gómez-Morán, A., Schreiber, M. R., et al. 2012, MNRAS, 419, 806

Roederer, I. U., Preston, G. W., Thompson, I. B., et al. 2014, AJ, 147, 136

Skrutskie, M. F., Cutri, R. M., Stiening, R., et al. 2006, AJ, 131, 1163

Smith, J. C., Stumpe, M. C., Van Cleve, J. E., et al. 2012, PASP, 124, 1000

Sneden, C., Preston, G. W., & Cowan, J. J. 2003, ApJ, 592, 504

Stumpe, M. C., Smith, J. C., Van Cleve, J. E., et al. 2012, PASP, 124, 985

Szentgyorgyi, A. H., & Furész, G. 2007, RMxAC, 28, 129

Tajitsu, A., Aoki, W., & Yamamuro, T. 2012, PASJ, 64, 77

Tauris, T. M., & Savonije, G. J. 1999, A&A, 350, 928

Tauris, T. M., & van den Heuvel, E. P. J. 2014, ApJL, 781, L13

Tremblay, P.-E., Bergeron, P., & Gianninas, A. 2011, ApJ, 730, 128

van Kerkwijk, M. H., Rappaport, S. A., Breton, R. P., et al. 2010, ApJ, 715, 51

Verbunt, F., & Rappaport, S. 1988, ApJ, 332, 193

Vos, J., Zorotovic, M., Vučković, M., Schreiber, M. R., & Østensen, R. 2018, MNRAS, 477, 40

Winn, J. N. 2011, in Exoplanets, ed. S. Seager (Tucson, AZ: Univ. Arizona Press), 55

Yahalomi, D. A., Shvartzvald, Y., Agol, E., et al. 2019, ApJ, 880, 33

Yee, S. W., Petigura, E. A., & von Braun, K. 2017, ApJ, 836, 77

Zhang, X. B., Fu, J. N., Liu, N., Luo, C. Q., & Ren, A. B. 2017, ApJ, 850, 125